We are IntechOpen,
the world's leading publisher of
Open Access books
Built by scientists, for scientists

6,900
Open access books available

186,000
International authors and editors

200M
Downloads

Our authors are among the

154
Countries delivered to

TOP 1%
most cited scientists

12.2%
Contributors from top 500 universities

CLARIVATE ANALYTICS
BOOK CITATION INDEX
INDEXED

WEB OF SCIENCE™

Selection of our books indexed in the Book Citation Index
in Web of Science™ Core Collection (BKCI)

Interested in publishing with us?
Contact book.department@intechopen.com

Chapter

Bismuth Telluride Solubility Limit and Dopant Effects on the Electronic Properties of Lead Telluride

Dana Ben-Ayoun and Yaniv Gelbstein

Abstract

The demand for energy efficiency has motivated many researchers to seek for novel methods capable of enhancing the conversion of heat to electricity. Most of the recently published methods for thermoelectric (TE) efficiency enhancement discuss on the reduction of the lattice thermal conductivity, with a minor focus on improved electronic optimization. This is attributed mainly to the fact that the electronic properties are correlated and opposing each other upon increasing the carrier concentration. It has been reported that the system of PbTe-BiTe has potentially high TE performance; this chapter is focused on a detailed investigation of the co-effect of bismuth as an effective electronic dopant and at the same time, as a second phase promoter in the PbTe matrix. $(PbTe)_x(BiTe)_{1-x}$ alloys were thermoelectrically examined and the values were analyzed analytically by the general effective media (GEM) approach.

**Keywords:** thermoelectric, PbTe, BiTe, solubility, GEM

1. Introduction

In the past decades, global climate changes, caused by combustion of fossil fuels and greenhouse gases emission, became a major environmental concern, accompanied with the dilution of conventional energy resources, raising the need for a renewable energy alternatives. Thermoelectricity dealing with this concern, is based on a direct conversion of waste heat into usable electrical energy; even a partial conversion of this waste heat will get us one step closer toward a cleaner and greener world. This goal has been achieved by thermoelectric converters and successfully initiated by the development of various highly efficient thermoelectric material classes. Such materials require a unique combination of the electrical and lattice properties (Seebeck coefficient (α), electrical resistivity (ρ), electronic thermal conductivity (κ_e), and lattice thermal conductivity (κ_l)), enabling the highest possible thermoelectric figure of merit values $ZT = \alpha^2 T/[\rho(\kappa_e + \kappa_l)]$, where T is the absolute temperature, for achieving significant conversion efficiencies. Since the electronic properties are strongly interdependent and follow opposite trends (α and ρ are decreased, and κ_e is increased) upon increasing the carrier concentration, most of the published studies were mainly focused on applying advanced nano-structuring approaches for κ_l reduction.

In the case of IV–VI-based chalcogenides and their alloys (known as among the most efficient thermoelectric alloys for intermediate working temperatures of up to 600°C) such nano-structuring approaches resulted in a significant increase of *ZT* up to ~2.5, due to an effective scattering of phonons without adversely affecting the electronic properties [1]. Yet, it is worth mentioning that such approaches already succeeded in reaching ultralow thermal conductivity [2], lightening the fact that other approaches, related to electronic optimization of chalcogenides for further enhancement of *ZT*, are still required.

Among the IV–VI-based chalcogenides, lead telluride is one of the most commonly used thermoelectric materials, but the maximal *ZT* achieved is only ~0.8 [3] which is still insufficient for converters in widespread industrial use. While thermoelectric properties are dependent on the carrier concentration, materials with carrier concentration higher than 10^{19} cm^{-3} are required. For undoped lead telluride, the change in the carrier concentration and carrier type is obtained by a method that enables the stoichiometry to be changed through thermal annealing in a Pb-rich (for *n*-type conductivity) or Te-rich (for *p*-type conductivity). One of the key methods for optimizing the electronic properties of these materials is by adding doping elements to the melt, while the most universally recognized lead telluride dopant is bismuth; it allows obtaining such carrier concentrations that can provide applicative values of thermoelectric conversion efficiency. The thermoelectric properties of the compounds in the system have been investigated, the processes taking place upon increasing the dopant concentration was also studied, but such researches were mainly focused on compositions within the solid solution up to the theoretical solubility limit [4, 5].

This present work, considering our synthesis process, investigates the bismuth effects in the matrix, beneath and beyond the solubility limit, as an effective electronic dopant yet at the same time, as a second phase promoter in the PbTe matrix. Moreover, to the best of our knowledge, most of the previous researches did not investigated the individual electronic contributions of the involved secondary phases embedded in the matrix on the effective thermoelectric transport properties. The general effective media (GEM) approach [6] enables to estimate the transport properties based on experimentally measured properties of each of the involved phases. Since the approach is taking into consideration geometrical aspects, it can be utilized for maximizing the thermoelectric figure of merit of composite materials by artificial alignment of the embedded secondary phase in the composite.
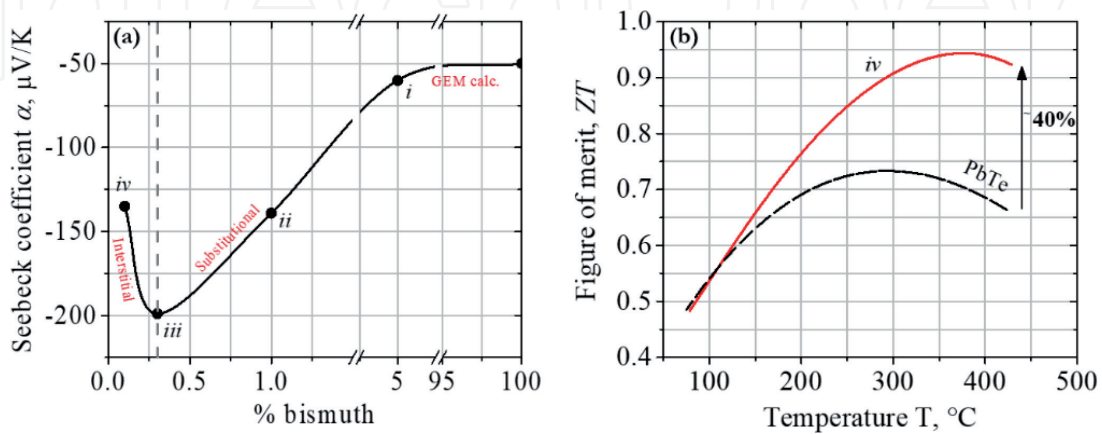
Figure 1.
(a) Bismuth concentration dependence of the room temperature Seebeck coefficient, α, scheme demonstrating the interstitial to substitutional pattern dissolution limit (at ~0.3%) which continues with the GEM calculations for two phase composites consisting an increasing amount of embedded metallic secondary phase. (b) The enhancement of the figure of merit, ZT, in the system along most of the temperature range required for practical operation.

Figure 1a shows the high potential of compositions with low amount of bismuth content, in the vicinity of the solubility limit, to attain high absolute Seebeck coefficient values. **Figure 1b**, demonstrates the potential to enhance the thermoelectric conversion efficiency while considering the co-effect of bismuth as an electronic donor dopant and as a secondary phase promoter in PbTe.

2. Experimental

Three $(PbTe)_x(BiTe)_{1-x}$ alloys, with different x values (**Table 1**), were synthesized from pure elements (5 N), mixed in the right stoichiometric ratio, and sealed in evacuated quartz ampoules under vacuum of 10^{-6} Torr. The ampoules were placed in a rocking furnace (Thermcraft Inc., Winston Salem, NC, USA) at 1000°C for 15 minutes, then water quenched. The cast ingots were milled to a maximal powder particle size of ~250 μm using agate mortar and pestle. The sieved powder was hot pressed (HPW5 Hot Press, FCT System GmbH, Rauenstein, Germany) under a mechanical pressure of 21 MPa at 730°C for 30 minutes under argon atmosphere, resulting in high density values of >98% of the theoretical density.

The thermoelectric transport properties of each alloy were measured up to 450°C as follows. The Seebeck coefficient, α, and electrical resistivity, ρ, were determined using the four-point probe method (Linseis LSR-3/800 Seebeck coefficient/electrical resistance measuring system). The thermal diffusivity, γ, was determined using the flash diffusivity method (LFA 457, NETZSCH). The total thermal conductivity, κ, was calculated using $\kappa = \gamma \cdot C_P \cdot \delta$, where C_P is the specific heat which was determined using differential scanning calorimetry (DSC 404, NETZSCH), and δ is the density of the sample measured using Archimedes method.

The crystal structure of the alloys was analyzed by X-ray powder diffraction (Rigaku DMAX 2100 powder diffractometer). The microstructure of the alloys was observed using scanning electron microscopy (SEM, JSM-5600, JEOL, Akishima, Japan) equipped with a backscattered electron detector. The chemical composition was measured using an energy-dispersive X-ray spectroscopy (EDS).

| Alloy	Bi [%at]	Matrix
i	5%	$(PbTe)_{0.95}(BiTe)_{0.05}$
ii	1%	$(PbTe)_{0.99}(BiTe)_{0.01}$
iii	0.3%	$(PbTe)_{0.997}(BiTe)_{0.003}$
iv	0.1%	$(PbTe)_{0.999}(BiTe)_{0.001}$

Table 1.
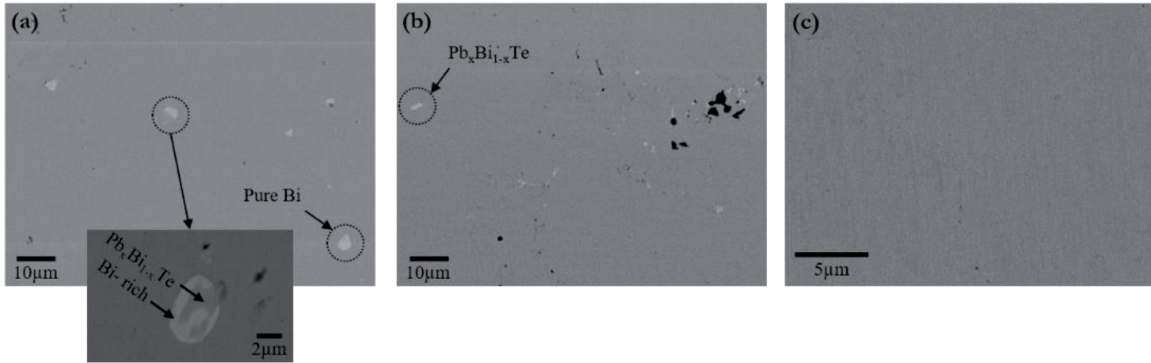*The investigated alloys notations.*

3. Results and discussion

PbTe has a NaCl cubic crystal structure with space group Fm-3m, melts congruently at 924°C [7]; BiTe has a BiSe trigonal crystal structure with space group P-3m1, consists of 12 close-packed layers along the c axis, melts at 540°C [8].

As can be seen by the XRD diffractogram presented in **Figure 2a**, the reflections are all belong to the lead telluride matrix in the rock salt structure, with no evidence of other phase's peaks. A reason for that might be that the amount of the second phase precipitants detected in the SEM analysis (**Figure 3a** and **b**) is clearly less than the detection limit of the XRD analysis.
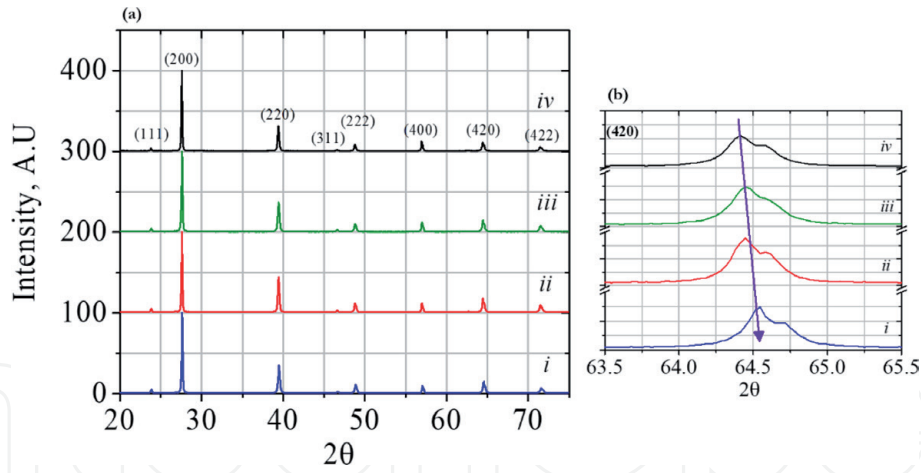
Figure 2.
(a) XRD diffractogram of the investigated i, ii, iii, and iv alloys and (b) a magnification of the (420) reflection at ~64°, indicating a volume decrease upon increasing the bismuth content.

Figure 3.
BSE-SEM micrographs of the investigated (a) i, (b) iii, and (c) iv alloys indicating in the inset the compositional modulations.

As shown in **Figure 2b**, with increasing the bismuth content in the lead telluride matrix, the peaks are constantly shifted toward higher angles, reflecting a constant decrease in the lattice parameter. This may be related to the fact that Bi^{3+} has lower ionic radius (1.03 A [9]) compared to the ionic radius of Pb^{2+} (1.19 A [9]), while bismuth substitutes lead in the NaCl structure. Moreover, it is well known that introducing bismuth to the PbTe matrix creates cation vacancies, which might also contribute to the decrease in lattice parameter while releasing internal stresses/lattice strains. Although broadening of the peaks due to lattice internal stresses caused by bismuth interstitial atoms would be expected, it was not observed in the investigated samples, probably due to the fact that the amount of bismuth at alloy *iv* is too small to affect the lattice.

Back-scattered electrons SEM micrographs of the investigated alloys are presented in **Figure 3a–c**. In **Figure 3a** of the investigated alloy *i*, compositional modulations reveal bright bismuth precipitants along with precipitants composed of several compositions. Since the contrast in back-scattered electrons SEM micrographs is correlated directly to its atomic number, it is obvious that the brighter the phase, the more bismuth it contains; thus, the precipitants contain a PbBiTe ternary phase surrounded by a brighter bismuth-rich phase. In alloy *iii*, PbBiTe ternary phase precipitant can be also detected (**Figure 3b**). The exact composition of the ternary phases, in both samples, could not be defined using EDS analysis. For alloy *iv*, a single-phase matrix, without any precipitant was detected, indicating a full solubility of the elements as can be seen in the representative micrograph in **Figure 3c**.

The logic behind this is that, at alloy *iv*, the dissolution pattern is by interstitial occupation mechanism. It is assumed that bismuth occupation in interstitial sites is less preferred with increasing the bismuth content (*iii*) → (*i*), and the dissolution pattern changes to a substitutional pattern (in line with XRD diffractograms shift, described above); the tendency to participate as a second phase is growing and its effect on the transport properties can be explained by the percolation theory as described by Rogacheva et al. [10]. Upon increasing the bismuth content, percolation passages are formed, causing spatial redistribution of the impurity atoms by self-interaction. By further introduction of bismuth to the matrix, bismuth clusters are formed. Taking the above into consideration, it is reasonable to assume that with increasing the amount of bismuth impurity in the matrix, the probability to form pure bismuth precipitants is growing. Moreover, the high number of ternary compounds existing in bismuth rich PbBiTe system [11], is an indication of a relatively easy restructuring of the lattice. We assume that the precipitant modulations observed might be a result of complexes formation whose composition corresponds to the composition of intermediary phases [10]. Overall, the system is influenced by the percolation effects, and goes through intermediate processes of complex and intermediate structure formations, that can give a reasonable explanation for the observations.

The Seebeck coefficient α, electrical resistivity ρ, thermal conductivity κ and figure of merit ZT, for the investigated alloys are presented in **Figure 4a–d**.

The Bi^{3+} tendency to substitute Pb^{2+} creates one free electron, a fact which obviously affect the electronic properties of the materials. The Seebeck coefficient at room temperature for alloy *i* ($-55 \, \mu VK^{-1}$) indicates the large amount of bismuth introduction to the PbTe matrix; the precipitants acting as a secondary metallic phase, enhancing the carrier concentration. Decreasing the bismuth concentration (alloys *ii* and *iii*) resulted in a gradual improvement of the Seebeck coefficient (-140 and $-200 \, \mu VK^{-1}$, respectively); a dramatic expected change when
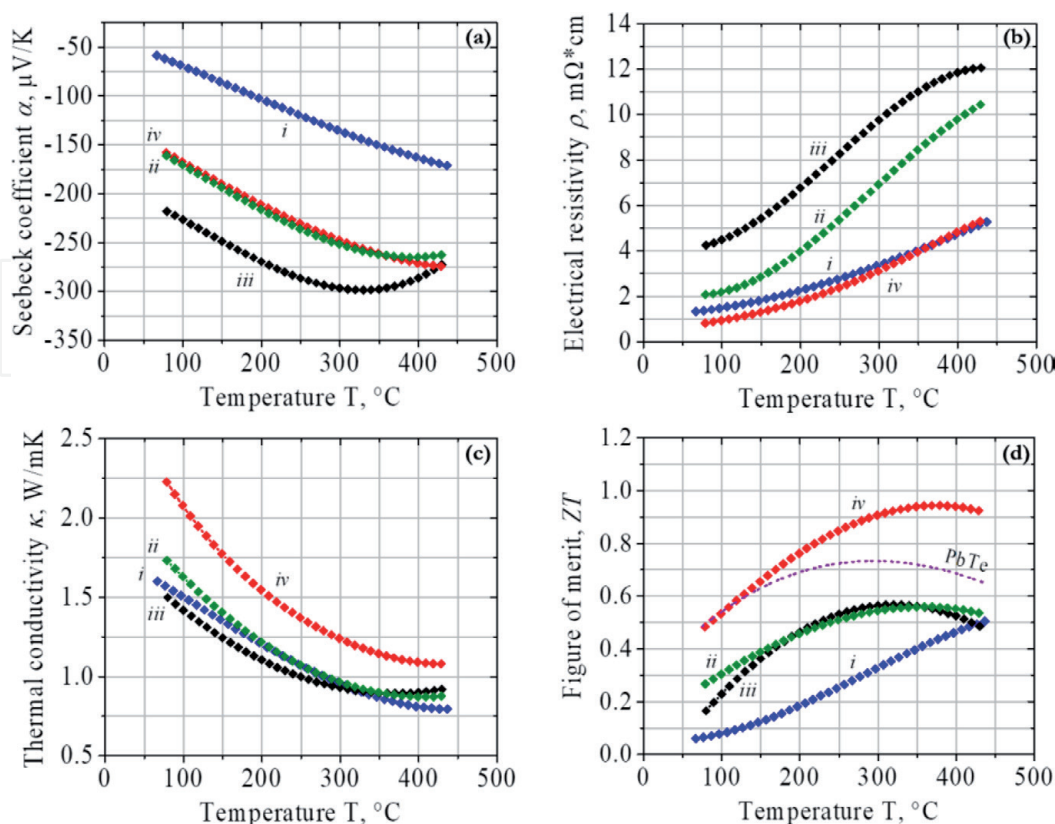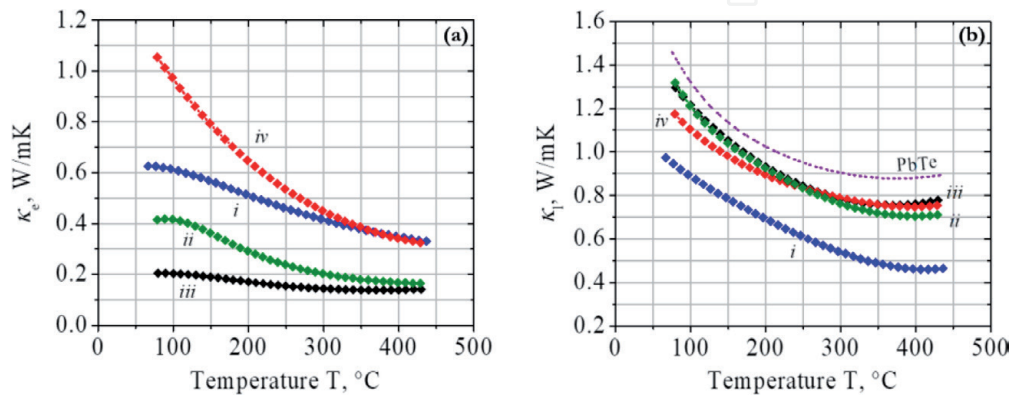

Figure 4.
Temperature dependence of (a) Seebeck coefficient, (b) electrical resistivity, (c) thermal conductivity, and (d) the thermoelectric figure of merit for the investigated i, ii, iii, and iv alloys.

considering the decreased metallic secondary phase amount. By further decreasing the bismuth content (alloy *iv*), the absolute Seebeck coefficient decreased ($-135 \, \mu VK^{-1}$). As can be seen in **Figure 3c**, there is full solubility of bismuth in the PbTe matrix; considering that fact, the reason for the unexpected behavior of Seebeck coefficient might be plant in the dissolution pattern changes as a function of bismuth content. As described above, at low amounts of bismuth, as in alloy *iv*, the dissolution pattern changed to interstitial pattern, where the bismuth electronic activity is relatively low. In that context, a maximum in the absolute Seebeck coefficient values can be reached in the vicinity of the bismuth concentration of alloy *iii*, where the threshold for the substitutional dissolution pattern is reached and it changes to interstitial pattern.

A similar trend observed in **Figure 4b**, from (*i*) → (*iii*), can be seen in the electrical resistivity values. This behavior supports the theory above and is attributed to the increased metallic contribution of the precipitates. Yet, one must keep in mind that bismuth impurities and precipitants cause defect formation in the crystal lattice which consequently scatter the charge carriers and increase the electrical resistivity. While comparing alloy *ii* and *iv*, the increased electrical resistivity in alloy *ii* is attributed to the low mobility due to charge carriers scattering. Moreover, the overlapping between the curves of alloys *i* and *iv* is attributed to the fact that in alloy *i* the charge carrier concentration is relatively high compared to alloy *iv*, while at the same time, in alloy *i* the mobility of the charge carriers is relatively low compared to alloy *iv*. In the last case, these two effects compensate each other and overall, they are affected by the bismuth both as a donor and as a precipitant initiator.

Since the thermal conductivity is affected both by bismuth as an effective electronic donor, but also as a phonon scatter source, both contributions were analyzed. The electronic contribution to the thermal conductivity, as shown in **Figure 5a**, was analyzed using Wiedemann-Franz relation, $\kappa_e = L \, \rho^{-1} \, T$, where L is the Lorentz constant equal to $2.45 \cdot 10^{-8} \, W\Omega K^{-2}$ calculated in a previously described procedure [12], ρ is the measured electrical resistivity (**Figure 4b**), and T is the absolute temperature. κ_e values follow the expected similar but opposite trends to the ρ values. The lattice contribution to the thermal conductivity, as shown in **Figure 5b**, was calculated by subtracting the calculated κ_e out of the measured κ_{tot} (**Figure 4c**); the gradual change in the κ_l as a function of bismuth content is associated with the cation vacancies described before for *iv*, and continues with increased lattice defects, created by the gradually phase separation observed in **Figure 3a–b**, acting as a phonon scattering source. The overlapping curves can be explained by the fact that the phase separation shown in *iii* (**Figure 3b**) is minor thus might affect κ_l in a very small manner, within

Figure 5.
Temperature dependence of the (a) electronic contribution and (b) lattice contribution to the thermal conductivity of the investigated alloys.

the measurement error of the curves. Overall the results indicate a reduction of ~20 and ~44% upon increased doping compared to pristine PbTe.

It is noted that the dominant thermal conduction mechanism is a bit different between the alloys. While alloys *i* and *iv* are affected by both lattice and charge carrier thermal conductions in the same manner, since their contributions are in the same order of magnitude, alloys *ii* and *iii* charge carrier thermal conduction is very low. This fact opens a window of opportunities for a possible further *ZT* enhancement by reducing the precipitants (observed in **Figure 3b**) size into the nano-scale for reduction of κ_l.

While combining both the thermal and electrical contributions to the thermo-electric efficiency (**Figure 4d**) it can be concluded that at 450°C, ~40% improvement compared to pristine PbTe was obtained; improvement that is attributed to an optimization between both bismuth contributions as an effective electronic dopant and as a second phase initiator.

In order to further investigate the electronic contribution of the secondary phase due to the geometrical morphology and amount, the general effective media (GEM) approach was applied [6]. The effective thermoelectric transport properties, for composite materials consisting of two separate phases, were calculated based on the effective thermal conductivity, κ_{eff}, and effective electrical resistivity, ρ_{eff}, calculated using Eq. (1) and the effective Seebeck coefficient, α_{eff}, using Eq. (2) [13].

$$x_1 \cdot \frac{(\sigma_1, \kappa_1)^{\frac{1}{t}} - (\sigma_{eff}, \kappa_{eff})^{\frac{1}{t}}}{(\sigma_1, \kappa_1)^{\frac{1}{t}} + A \cdot (\sigma_{eff}, \kappa_{eff})^{\frac{1}{t}}} = (1 - x_1) \cdot \frac{(\sigma_{eff}, \kappa_{eff})^{\frac{1}{t}} - (\sigma_2, \kappa_2)^{\frac{1}{t}}}{(\sigma_2, \kappa_2)^{\frac{1}{t}} + A \cdot (\sigma_{eff}, \kappa_{eff})^{\frac{1}{t}}} \tag{1}$$

$$\frac{\alpha_{eff} - \alpha_2}{\alpha_1 - \alpha_2} = \frac{\frac{\frac{\kappa_{eff}}{\kappa_2}}{\frac{\sigma_{eff}}{\sigma_2}} - 1}{\frac{\frac{\kappa_1}{\kappa_2}}{\frac{\sigma_1}{\sigma_2}} - 1} \tag{2}$$

Where α_1, ρ_1, κ_1 represent the secondary phase embedded in the matrix; α_2, ρ_2, κ_2, represent the matrix; x_1 and $(1 - x_1)$ represent the relative amounts of each of the phases; t represent the homogenous level of distribution of the secondary phase in the matrix, while $t = 1$ stands for an even distribution [14, 15]; A represents the morphological alignment and ranges from "series" (for $A = 0$) to "parallel" (for $A = \infty$) relative to the electrical potential or temperature gradients, while $A = 2$ corresponds to a spherical morphology of the secondary phase [14, 15]. By applying the GEM approach to the investigated case of an embedded bismuth secondary phase inside alloy *iii* matrix, the applied transport properties were the reported values for pure bismuth (−50 μVK^{-1} [16], 0.129 mΩ cm, and 7.97 W mK^{-1} at room temperature [17]) and the experimental data for alloy *iii* at room temperature (**Figure 4a–c**). A was chosen to be equal to different morphological alignment conditions, represented by 0, 2, 8 and infinity.

Using the above data, the effective thermoelectric transport properties, shown in **Figure 6a–d**, were calculated. The measured room temperature experimental values for our *i* and *ii* investigated alloys, are shown in **Figure 6** as black stars; taking into consideration the 10% measurement error, they follow the curve which represent infinitesimal A and uneven distribution of the phase ($t \neq 1$). The conclusion is in line with **Figure 3a–b**, where the precipitants location is mainly in the grain boundary, forcing an elongated shape for the most of them.

As been presented in the experimentally measured values (**Figure 4a–c**), and is in agreement with previously reports, in low amounts of bismuth in the matrix the transport properties are acting abnormally, with regard to the changing pattern of dissolution, up to a point where the dissolution pattern remains steady. Above that
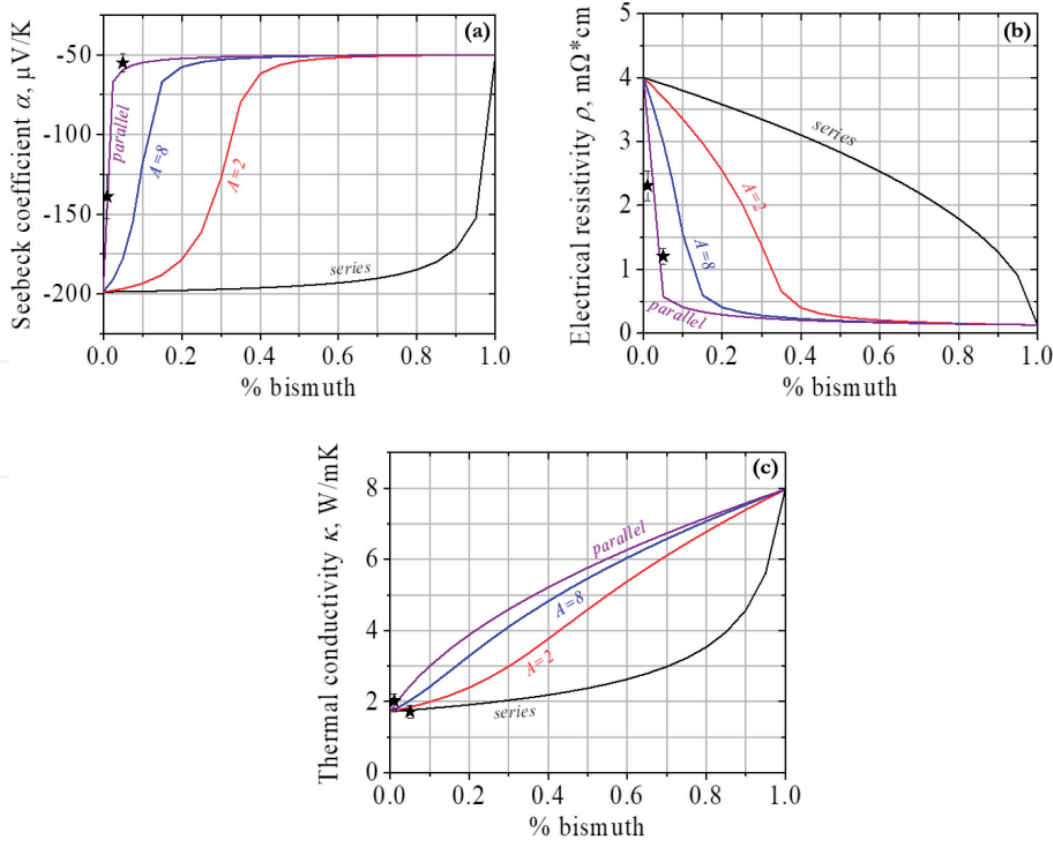
Figure 6.
Calculated GEM curves at room temperature of (a) effective Seebeck coefficient, (b) effective electrical resistivity and (c) effective thermal conductivity as a function of the embedded bismuth percentage, under different morphological alignment and uneven distribution conditions (t = 0.5).

level, the GEM evaluation can predict the transport properties in a very reliable way, since the transport properties of the composite are expected to act as a composite with an increasing amount of a secondary metallic phase.

In our homogeneous distribution level and morphological alignment conditions, it can be seen that up to 0.1%, a slight change in bismuth concentration is accompanied with a drastic change in the electronic properties of the composite. A drastic degradation in the absolute Seebeck coefficient along with a great improvement in the electrical conductivity, sums up in an increased power factor ($\alpha^2\rho^{-1}$); yet while considering the thermal conductivity increment, the overall room temperature thermoelectric efficiency is decreased. On the other hand, the "series" morphological alignment condition at room temperature, exhibits more moderate changes that might allow bigger introduction of bismuth to the matrix, which will reduce the lattice contribution to the thermal conductivity, and at the same time will not affect as drastically the electronic properties. This finding implies on a potential method for enhancing the thermoelectric efficiency by an artificial "series" morphological alignment of the secondary phase which can lead to possible further study.

The reason for the small mismatches observed in our GEM calculations, might be related to the fact that the matrix was represented by alloy *iii*; it is well known that even a slight change in impurity content, affect substantially the transport properties.

4. Conclusions

The co-effect of bismuth as an effective electronic dopant and at the same time, as a second phase promoter in the PbTe matrix was investigated and explained in details with regard to the dissolution pattern transition. These two effects on the

thermoelectric properties were demonstrated and resulted in a ~40% *ZT* enhancement compared to the pristine PbTe. The GEM analysis of composites with an increased amount of precipitates paved a potential route for further enhancement of the thermoelectric efficiency upon an artificial serial alignment of the embedded secondary phase in the composite.

Acknowledgements

Conflict of interest

The authors declare no conflict of interest.

Author details

Dana Ben-Ayoun* and Yaniv Gelbstein
Department of Materials Engineering, Ben-Gurion University of the Negev,
Beer-Sheva, Israel

*Address all correspondence to: danabenayoun@gmail.com

IntechOpen

References

[1] Hazan E, Madar N, Parag M, Casian V, Ben-Yehuda O, Gelbstein Y. Effective electronic mechanisms for optimizing the thermoelectric properties of GeTe-rich alloys. Advanced Electronic Materials. 2015;**1**(11):1-7

[2] Xu B, Feng T, Agne MT, Zhou L, Ruan X, Snyder GJ, et al. Highly porous thermoelectric nanocomposites with low thermal conductivity and high figure of merit from large-scale solution-synthesized $Bi_2Te_{2.5}Se_{0.5}$ hollow nanostructures. Angewandte Chemie, International Edition. 2017;**56**(13):3546-3551

[3] Komisarchik G, Gelbstein Y, Fuks D. Solubility of Ti in thermoelectric PbTe compound. Intermetallics. 2017;**89**:16-21

[4] Zhu P, Imai Y, Isoda Y, Shinohara Y, Jia X, Zou G. Composition-dependent thermoelectric properties of PbTe doped with Bi_2Te_3. Journal of Alloys and Compounds. 2006;**420**(1-2):233-236

[5] Christakudi TA, Christakudis GC, Borissova LD. Thermoelectric power of solid solutions $(PbTe)_{1-x}(Bi_2Te_3)_x$ with $0 \leqq x \leqq 0.02$. Physica Status Solidi. 1995;**190**(2):537-544

[6] Gelbstein Y. Simulation of morphological effects on thermoelectric power, thermal and electrical conductivity in multi-phase thermoelectric materials. In: Skipidarov S, Nikitin M, editors. Thermoelectrics for Power Generation. London, UK: IntechOpen; 2016. pp. 286-301

[7] Noda Y, Ohba S, Sato S, Saito Y. Charge distribution and atomic thermal vibration in lead chalcogenide crystals. Acta Crystallographica Section B. 1983;**39**(3):312-317

[8] Shimazaki H, Ozawa T. BiTe, a new mineral from the Tsumo mine, Japan. American Mineralogist. 1978;**63**:1162-1165

[9] Shannon R. Revised effective ionic radii and systematic studies of interatomie distances in halides and chaleogenides. Acta Crystallographica. 1976;**A32**:751-767

[10] Rogacheva E, Vodorez O, Pinegin V, Nashchekina O. Evidence for self-organization processes in PbTe-Bi_2Te_3 semiconductor solid solutions. Journal of Materials Research. 2011;**26**(13):1627-1633

[11] Karpinskii OG, Shelimova LE, Avilov ES, Kretova MA, Zemskov VS. X-ray diffraction study of mixed-layer compounds in the PbTe-Bi_2Te_3 system. Inorganic Materials. 2002;**38**(1):17-24

[12] Gelbstein Y, Dashevsky Z, Dariel MP. High performance *n*-type PbTe-based materials for thermoelectric applications. Physica B: Condensed Matter. 2005;**363**(1-4):196-205

[13] Gelbstein Y. Phase morphology effects on the thermoelectric properties of $Pb_{0.25}Sn_{0.25}Ge_{0.5}Te$. Acta Materialia. 2013;**61**(5):1499-1507

[14] Bergman DJ, Levy O. Thermoelectric properties of a composite medium. Journal of Applied Physics. 1991;**70**(11):6821-6833

[15] Webman I, Jortner J, Cohen MH. Thermoelectric power in inhomogeneous materials. Physical Review B. 1977;**16**(6):2959-2964

[16] Goldsmid H. Bismuth-antimony alloys. Physica Status Solidi. 1970;**7**:7-28

[17] Khalouk K, Chaib C, Gasser J-G. Electrical and thermal conductivities and Seebeck coefficient of liquid copper-bismuth alloys. Philosophical Magazine Letters. 2009;**89**(3):249-262